

Constraints on the Strength of the Upper Crust from Stress Inversion of Fault Slip Data

ZE'EV RECHES

Department of Geology, Hebrew University, Jerusalem, Israel

GIDON BAER AND YOSSEF HATZOR¹

Geological Survey of Israel, Jerusalem, Israel

The coefficient of friction of small faults in the field are estimated here by stress inversion of fault slip data. The small faults that were measured in Israel and the Grand Canyon, Arizona, are considered as representing natural friction experiments. The stresses associated with the faulting are determined by a stress inversion method which incorporates the Coulomb failure criterion [Reches, 1987]. The coefficients of friction determined for 27 fault clusters in limestone, sandstone, and basalt range from 0.0 to 1.3 with mean value of 0.58 ± 0.37 . These values are in general agreement with the friction of 0.6–0.85 determined from laboratory experiments. The magnitudes of the calculated principal stresses are compared with in situ stress measurements in similar tectonic environments.

INTRODUCTION

The gross strength of rocks in the crust is bounded by the frictional resistance to slip along fractures because this resistance is usually smaller than the strength of intact crustal rocks. Thus crustal strength is commonly estimated from values of the friction determined in laboratory experiments [Brace and Kohlstedt, 1980]. Byerlee [1978] demonstrated that the frictional resistance to slip in laboratory experiments, in general, is not dependent on rock type, temperature and strain rate. He showed that slip along an existing fracture occurs when

$$\tau = A \sigma_n + B \quad (1)$$

where τ and σ_n are the shear and normal stresses acting on the fracture and A and B are constants. This equation is essentially the Coulomb failure criterion in which A is the friction coefficient and B is the cohesion. Byerlee also showed that in many experiments

$$A = 0.85 \quad B = 0 \quad \text{for } 3 < \sigma_n < 200 \text{ MPa} \quad (2a)$$

$$A = 0.6 \quad B = 60 \pm 10 \quad \text{for } \sigma_n > 200 \text{ MPa} \quad (2b)$$

Brace and Kohlstedt [1980] referred to (1) and (2) as Byerlee's law and utilized them to evaluate the strength of the upper crust. Brace and Kohlstedt [1980, equation (3)] assumed that slip occurs when the tectonic stresses satisfy (1) along the most favorably oriented fractures and showed that the crustal strength is

$$(\sigma_1 - \sigma_3) \approx 4\sigma_3 \quad \text{for } \sigma_3 < 110 \text{ MPa} \quad (3a)$$

$$(\sigma_1 - \sigma_3) \approx 3.1 \sigma_3 + 210 \quad \text{for } \sigma_3 > 110 \text{ MPa} \quad (3b)$$

The predictions of (3) appear to bound the results of in situ stress measurements [McGarr and Gay, 1978; Brace and Kohlstedt, 1980],

¹ Also at Department of Geology, Hebrew University, Jerusalem, Israel. Now at Department of Civil Engineering, University of California, Berkeley.

Copyright 1992 by the American Geophysical Union.

Paper number 90JB02258.
0148-0227/92/90JB-02258\$05.00

and thus Byerlee's law became a widely used criterion for crustal strength.

Raleigh *et al.* [1972] measured the in situ stresses and pore fluid pressure at Rangely, Colorado, and found that these in situ conditions fit well the friction coefficient of 0.81 measured in the laboratory for the local Weber sandstone. In general, however, measurement of the friction coefficient in the field is complicated and expensive, and thus it is rarely done.

Our main objective here is to estimate the in situ friction coefficients by stress inversion of fault slip data measured in the field. The present approach is to inspect small faults in the field as if they are the outcome of natural friction experiments. A single fault provides limited information on tectonic stresses and friction; yet several faults which slipped under the same state of stress may constrain the stresses and the friction coefficients. We examine clusters of faults and calculate the stress tensor and the coefficient of friction which best fit simultaneous slip along the faults. We outline the main features of the present stress inversion [Reches, 1987], and the new improvements, including the procedure to estimate the coefficients of friction. The calculated friction values are then compared with Byerlee's law, and the calculated magnitudes of the principal stresses are compared with measured magnitude of in situ stresses.

STRESS INVERSION METHOD

Approach

Stress inversion methods are used to determine the state of stress which could cause slip along a group of faults measured in the field. Most stress inversion methods follow the assumption of Bott [1959] that slip along a fault occurs in the direction of the maximum resolved shear stress [e.g., Carey and Bruiner, 1974; Angelier, 1984; Ellsworth, 1982; Gephart and Forsyth, 1984; Michael, 1984]. These methods calculate the stress axes which minimize the angular deviation between the observed slip axis along a fault and the axis of the maximum resolved shear stress determined from the general stress. These inversion methods do not incorporate friction or cohesion. The inversion method of Reches [1987] which incorporates failure conditions, is based on the following assumptions:

1. The slip along a fault occurs in the direction of maximum re-

solved shear stress or, equivalently, normal to the axis of zero shear stress [Bott, 1959].

2. The shear and normal stresses on the fault satisfy the failure condition

$$|\tau| = \mu \sigma_n \tag{4}$$

where τ and σ_n are the magnitudes of the shear and normal stresses in the slip direction, and μ is the coefficient of friction. Cohesion and pore fluid pressure are not incorporated in the failure criterion for reasons discussed below.

3. The slip events occurred under relatively uniform conditions: the faults were active under the same state of stress and the friction of the faults can be represented by their mean values. It is also assumed that the amount of slip and rotations of the faults are small.

Assumptions 1 and 3 are common to all published stress inversion methods, whereas the failure criterion of assumption 2 is used in the present method. Assumption 2 is the Amonton's friction law (or Coulomb's criterion for no cohesion case). Jaeger and Cook [1976, p. 95] stated that "...the simplest and most important criterion (of faulting)....(was) introduced by Coulomb [1773]". This criterion is the most widely used criterion in soil and rock mechanics, the validity of which was demonstrated in countless experiments. The quantitative geophysical equivalent of this criterion is Byerlee's law, described above.

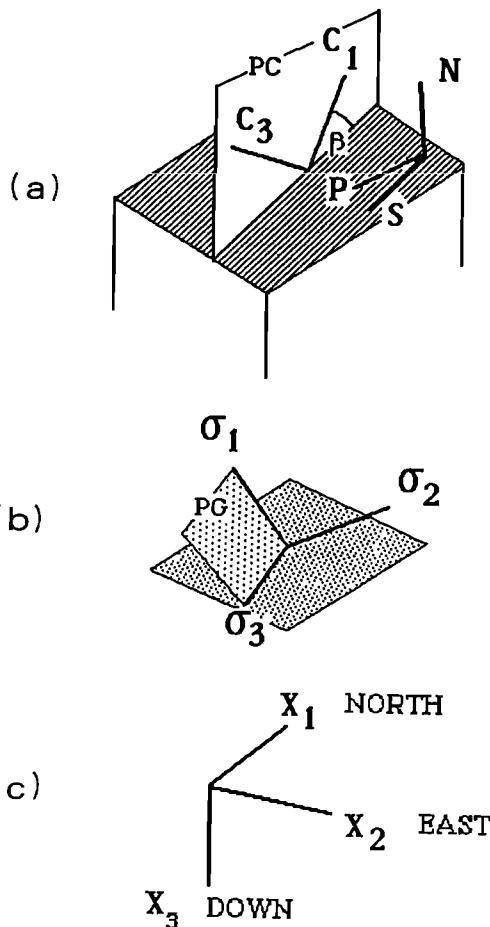


Fig. 1. Fault geometry and the stress tensors associated with the slip along it. (a) N, normal to fault; S, observed slip axis; C₁ and C₃, axes of the ideal tensor; P, axis of maximum resolved shear stress on the fault surface; β, angle between C₁ and S axis with the PC plane. (b) The axes of the general tensor, σ₁, σ₂, and σ₃, which satisfy slip along all faults; PG, the principal plane of σ₁-σ₃. (c) The coordinate system in field relation

The stress tensor is determined according to Reches [1987]. Each fault is represented by two unit vectors: one vector normal to the fault N_i, i=1, 2, and 3, and second vector parallel to the slip axis S_i, i=1, 2, and 3, where N_i and S_i are the directional cosines in an orthogonal coordinate system, X_i (Figure 1). It was chosen that X₁ is horizontal and pointing northward, X₂ is horizontal and pointing eastward, and X₃ points downward (Figure 1c). The unknown stress components in this coordinate system are σ₁₁, σ₂₂, σ₃₃, τ₂₃, τ₁₃, and τ₁₂ (pore pressure will be discussed below). The stress σ₃₃ is the overburden stress in the vertical direction.

Given S_i as the slip axis and B_i as the axis normal to it on the fault plane, then

$$B = N \times S,$$

where x indicates vector multiplication. By following the stress analysis of Jaeger and Cook [1976, chapter 2] and using the geometric relations between N_i and S_i, assumption 1 above becomes

$$(\sigma_{11} - \sigma_{33})N_1 B_1 + (\sigma_{22} - \sigma_{33})N_2 B_2 + \tau_{23}(N_2 B_3 + B_2 N_3) + \tau_{13}(N_1 B_3 + B_1 N_3) + \tau_{12}(N_1 B_2 + B_1 N_2) = 0 \tag{5a}$$

and assumption 2 becomes

$$(\sigma_{11} - \sigma_{33})N_1 S_1 + (\sigma_{22} - \sigma_{33})N_2 S_2 + \tau_{23}(N_2 S_3 + S_2 N_3) + \tau_{13}(N_1 S_3 + S_1 N_3) + \tau_{12}(N_1 S_2 + S_1 N_2) = \mu [(\sigma_{11} - \sigma_{33})N_1^2 + (\sigma_{22} - \sigma_{33})N_2^2 + \sigma_{33} + 2\tau_{23}N_2 N_3 + 2\tau_{13}N_1 N_3 + 2\tau_{12}N_1 N_2] \tag{5b}$$

By writing these two equations for each of the K faults in the studied set one obtains a system of 2K equations. This system is the matrix multiplication

$$A \times D = F \tag{6a}$$

where A is a 2K by 5 matrix, D is a vector of unknown stresses with five terms, and F is a vector with 2K terms. The vector D of the unknown stresses has the form

$$(\sigma_{11} - \sigma_{33}), (\sigma_{22} - \sigma_{33}), \tau_{23}, \tau_{13}, \tau_{12} \tag{6b}$$

The vector F has the form

$$0, 0, \dots, \sigma_{33}, \sigma_{33}, \dots \tag{6c}$$

where the first K terms are zero and the last K terms are σ₃₃.

The system A x D = F is an overdetermined linear system in which A and F are known for the measured fault and slip orientations. The stress vector D is determined by linear algebra methods, and a general tensor, σ₁, σ₂, and σ₃, with the smallest least squares error is calculated (Figure 1c).

The above procedure is repeated for friction coefficients ranging from 0.0 to 2.0; a separate stress tensor is determined for each coefficient of friction and a total of up to 20 different solutions for each cluster. A stress solution is regarded unacceptable if the calculated normal stresses across one or more faults are tensile. The reason for this rejection is that rocks subjected to tensile stresses (σ₃ < 0) yield by jointing and not by shear along faults.

Pore fluid pressure and cohesion. Incorporating pore fluid pressure and rock cohesion in the inversion analysis only slightly modifies the above equations; however, these parameters cannot be determined independently by the present method.

Equation (4) is modified to include cohesion C and pore pressure P_p,

$$|\tau| = C + \mu(\sigma_n - P_p) \tag{7}$$

Equation (5a) which represents the first assumption remains unchanged, whereas eq. (5b) which represents assumption 2, becomes

$$\begin{aligned}
 & (\sigma_{11} - \sigma_{33})N_1S_1 + (\sigma_{22} - \sigma_{33})N_2S_2 + \tau_{23}(N_2S_3 + S_2N_3) \\
 & \quad + \tau_{13}(N_1S_3 + S_1N_3) + \tau_{12}(N_1S_2 + S_1N_2) \\
 = P_c & + \mu[(\sigma_{11} - \sigma_{33})N_1^2 + (\sigma_{22} - \sigma_{33})N_2^2 + 2\tau_{23}N_2N_3 \\
 & \quad + 2\tau_{13}N_1N_3 + 2\tau_{12}N_1N_2] \quad (8a)
 \end{aligned}$$

where $P_c = C + \mu(\sigma_{33} - P_p)$. These changes lead to a change in the vector F (6c),

$$0, 0, \dots, 0, P_c, P_c, \dots, P_c \quad (8b)$$

where the first K terms are zero and the last K terms are P_c . P_c is the sum of three stress components: rock cohesion C , pore fluid pressure P_p , and vertical stress, σ_{33} . In the present formulation it is not possible to separate between these components. Thus we assume that slip occurred primarily along faults with vanishing cohesion, $C \approx 0$. The calculated stresses are presented by the ratio of the effective principal stresses,

$$\phi = (\sigma_1 - P_p) / (\sigma_{33} - P_p) \quad (9)$$

The usage of ratios of the effective stresses instead of using absolute values does not modify the stress orientations and the stress ratio ϕ .

Misfits and Selection Criterion

The solution of the linear system of equations (equations 5) provides a general stress tensor which can cause slip along all faults in the cluster. The quality of a particular solution should indicate the deviation between the properties of this general tensor and the field observations. We calculate and apply two types of deviations which are presented by angles of misfit as described below.

The principal axes misfit angle PAM. Slip along a fault which obeys Coulomb failure criterion may occur under many states of stress. However, the difference between the maximum and minimum principal stresses is minimized only for one orientation of the stress tensor [Jaeger and Cook, 1976, chapter 2]. This tensor of the least stress difference is defined as the ideal tensor, marked by C_1 and C_3 in Figure 1a. The principal stresses of the ideal tensor, C_1 and C_3 , are within a plane defined by the slip axis and the normal to the fault (Figure 1a); the C axis makes an angle of $\beta = 45^\circ - \theta/2$ with the slip axis and an angle of $45^\circ + \theta/2$ with the normal to the fault, where $\theta = \tan^{-1} \mu$, μ is the coefficient of friction.

The angles between the axes of the ideal tensor, C_1 , C_2 , and C_3 , and the axes of the general tensor, σ_1 , σ_2 , and σ_3 in Figure 1b, are calculated for each fault in the cluster. The mean misfit angle of the principal axes for a given fault is

$$t = (C_1 \wedge \sigma_1 + C_2 \wedge \sigma_2 + C_3 \wedge \sigma_3) / 3$$

where \wedge indicates the angle between the two axes. However, if the stress tensor is for axisymmetric conditions, for example, $\sigma_2 \approx \sigma_3$, large angles $C_2 \wedge \sigma_2$ and $C_3 \wedge \sigma_3$ do not necessarily indicate large angular deviation between the two tensors. To compensate for this effect, we redefine t as

$$t = [(1 - \phi) C_1 \wedge \sigma_1 + \phi C_3 \wedge \sigma_3] / 2$$

where $\phi = (\sigma_2 - \sigma_3) / (\sigma_1 - \sigma_3)$ is the stress ratio calculated by the stress inversion. In a case of small ϕ , the misfit will be determined primarily by the deviation of σ_1 axis, and vice versa for large ϕ . These variations agree with the implications of extreme ϕ : small ϕ indicate that any position within the principal plane normal to σ_1 could fit the σ_2 and σ_3 axes (typical triaxial test).

The mean misfit angle of all faults in the cluster is

$$PAM = \{ \sum t \} / K$$

where K is the number of faults. PAM is defined as the principal axes misfit angle.

The slip misfit SM. The slip misfit is the angle between the slip axis measured in the field (S in Figure 1a), and the direction of maximum resolved shear on the fault plane (P in Figure 1a). The direction of maximum resolved shear is calculated by substituting the general tensor and the observed attitude of the fault plane, into the equation of the shear stress acting on a plane. The slip misfit, SM , is the mean angle between the observed and calculated slip axes of all faults in the cluster.

Selection criterion. SM is less restricted than PAM and it may vanish for large number of general tensors. For example, if the plane common to σ_1 and σ_3 of the general tensor (PG in Figure 1b), coincides with the plane defined by the slip axis and the normal to the fault (PC in Figure 1a), SM vanishes for $0^\circ < \beta < 90^\circ$. On the other hand, under these conditions, PAM vanishes only for a unique orientation of $\beta = 45^\circ - \theta/2$. Thus the slip misfit angle is not directly constrained by the friction coefficient of the fault.

PAM appears to be a good criterion for selecting the best solution. It evaluates the accuracy of the solution by comparing the ideal tensor of each individual fault with the general tensor of the fault cluster. As the orientation of the ideal tensor depend on the coefficient of friction (angle β in Figure 1c), then PAM also depends on the coefficient of friction. Further, as the ideal tensor is unique for each given fault, the PAM angle is a constrained and conservative estimate of the misfit of the solution. For these reasons we used the principal axes misfit to select the best solution.

Confidence Margins

The confidence margins are evaluated here by sampling with replacement [Stuart, 1984], known also as bootstrapping [Efron, 1982; Michael, 1987]. As a measured cluster of faults is a finite sample from a large (infinite) population of faults, it is assumed that the parameters of the actual infinite population may be estimated by sampling with replacement. Stuart [1984, p. 29] stated that "Sampling with replacement is equivalent to sampling without replacement from a population of infinite size".

In the calculations the original cluster of K faults is resampled by random selection of additional samples, each with K faults. This implies that the additional samples may contain some of the original data more than once. The mean values of the additional samples have normal distribution about the true mean of the population regardless of the distribution of the original population [Stuart, 1984]. In a population with normal distribution, 31.63% of the solutions deviate by one standard deviation or more from the true mean. Thus, when 31.63% of cases which are farthest from the mean are deleted, the remaining 68.27% bound the confidence margins of ± 1 standard deviation about the mean.

Sampling with replacement was applied to the present inversion by the following procedure. First, the best fit solution and the corresponding friction coefficient are determined as described earlier. Second, the original cluster of faults is resampled by random selection to yield N additional samples. Each of these samples has the same number of faults as the original file; some of the faults are sampled more than once, while others are not sampled. Up to 500 additional samples are selected. Third, the stress inversion calculations are applied to all additional samples to generate N stress tensors. These calculations are performed for the friction coefficient determined earlier. Fourth, the mean stress axes are computed from the N solutions. The angular deviations between each of the three principal stress axes of each of the N tensors and the corresponding mean principal axes are computed. Fifth, 31.63% of the N solutions

TABLE 1. Fault Sets Used in the Present Analysis

Location	Faults		Rock type	Local Dip	Estimated Friction ^g	Comments
	Accept	Delete				
Gevanim Dome, Ramon						
West	16	2	LS ^a	12°	NA	Uniform set, poor friction estimate
Northwest I	18		LS ^a	20°	0.5	
II	8	4			NA	Uniform set, poor friction estimate
North I	25		LS ^a	50°	0.5	
II	10	5			1.3	
East I	15		LS ^a	27°	1.2	
II		15			NA	Poor stress solution
South I	13		LS ^a	40°	0.0	
II		8			NA	Poor stress solution
Afore	14		LS ^a	15°	0.5	
Saharonim Dome, Ramon						
West	22	2	LS ^a	35°	0.6	
North I	27	3	LS ^a	40°	0.5	
II	29	2			0.1	
Northeast	13	1	LS ^a	25°	0.6	
Southeast	16	1	LS ^a	24°	0.4	
Parsa	30	2	LS ^b	20°	1.1	
Palisades Monocline, Arizona						
GC166	6		LS ^c	2°	0.8	
GC172a	18	1	LS ^c	3°	0.6	
GC179	17		LS ^c	2°	0.6	
GC263403	56	2	SS ^d	15°	1.3	
GC412416	11	1	Bt ^e	3°	0.4	
Gilboa' Block, Israel						
Gid'ona 3	14	1	LS ^f	30°	0.4	
Gid'ona 4	13	1	LS ^f	22°	0.5	
Gid'ona 5	15	5	LS ^f	18°	0.2	
Bet-Alpha	12		LS ^f	40°	0.2	
Avinadav I	17		LS ^f	8°	1.0	
II	16	3	LS ^f	8°	0.0	
Total	451	59				
Mean friction					0.58 ± 0.37	

NA, not available

a, Triassic, Saharonim Formation.

b, Cenomanian, Hazera Formation.

c, Permian, Kaibab Formation.

d, Cambrian, Tapeats Sandstone.

e, Precambrian, Cardenas Lavas.

f, Eocene chalky limestone.

g, Estimates of friction coefficients according to principal axes misfit.

which are furthest from the mean solution are deleted; the remaining 68.27% solutions form the confidence margins of ± 1 standard deviation.

EXAMPLES OF FAULT SETS

We analyze 510 faults grouped in 27 clusters (Table 1). The faults in some adjacent field stations have been merged, whereas other stations were split into primary and secondary subsets. The data include the attitude of the fault plane and the slip axis and the sense of slip for each fault. Most of the analyzed faults were measured in limestone layers, some in sandstones and siltstones, and one station in basalt (Table 1); normal, strike-slip, oblique-slip and reverse faults are included.

Field Relations

Ramon Domes, southern Israel. Faults were measured in two elongated domes: Gevanim, a 4 km by 2 km dome, and Saharonim, a 2.4 km by 0.8 km dome (Figure 2a). These two structures are adjacent to the Ramon fault which is a major fault within the 400-km-

long Sinai-Israel shear belt. Triassic and Jurassic sedimentary rocks and Lower Cretaceous igneous intrusions are exposed in these domes. The structural analysis of the domes reveals the superposition of folding phases associated with compressive tectonic stresses, and doming associated with the emplacement of a shallow laccolithic intrusion [Baer and Reches, 1989]. Faults were also measured in two stations outside the domes, Afore and Parsa.

Palisades monocline, Grand Canyon, Arizona. The Palisades monocline is a branch of the 250 km long East Kaibab monocline of the Colorado Plateau (Figure 2b) [Reches, 1978]. This monocline formed during the Laramide deformation under regional tectonic compression. The compressive stresses reactivated and inverted the sense of slip along Precambrian faults in the Grand Canyon region. The Palisades monocline developed due to draping over the vertical Palisades fault and buckling due to the horizontal compression. Small faults were measured here in rocks ranging from the Cardenas Lavas of Precambrian age (1.2 b.y. old) to the Kaibab Limestone of Permian age.

The Gilboa' region, northern Israel. The Gilboa' is a 20 km by 20 km uplifted block on the western margins of the Dead Sea

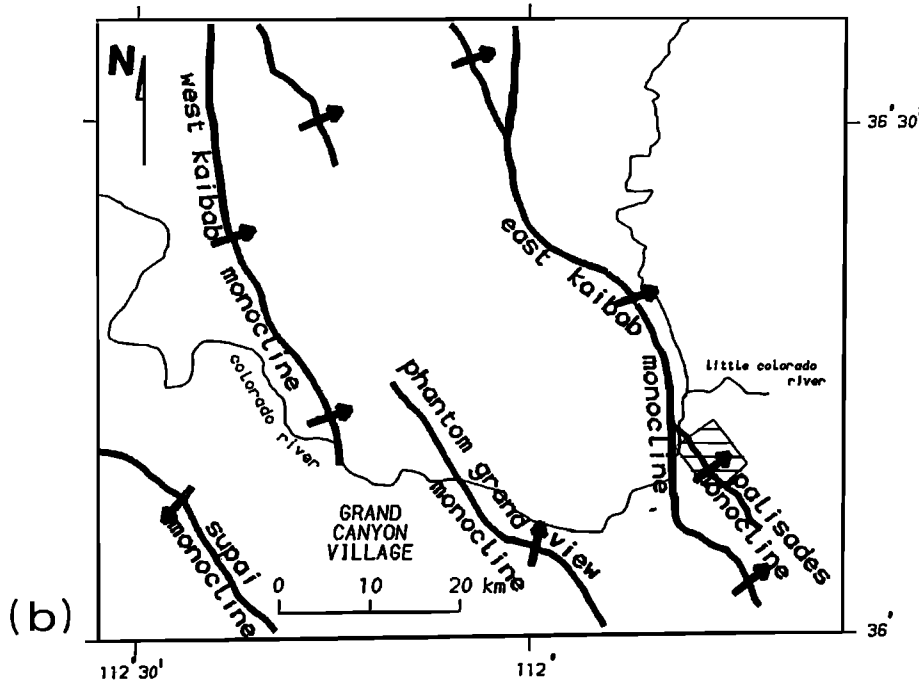
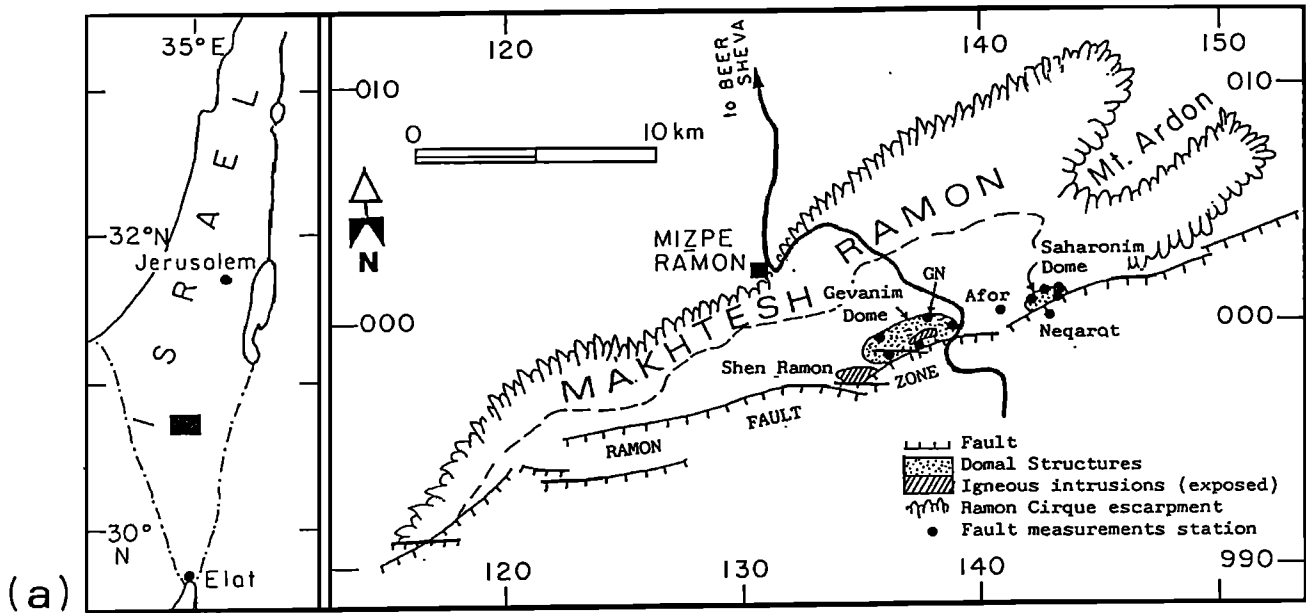


Fig. 2. Location maps for the field measurements. (a) Ramon area in southern Israel. Solid dots indicate sampling stations for the fault clusters [after Zak, 1968]. (b) The Palisades monocline, eastern Grand Canyon, Arizona. Solid rectangle indicate the sampling region [after Reches, 1978]. (c) The Gilboa' block, the margins of the Dead Sea rift, Israel [after Hatzor and Reches, 1990].

transform, with exposed rocks of Upper Cretaceous to Recent (Figure 2c). The eastern boundary of the block is delineated by faults of the Dead Sea rift, whereas the northern boundary of the block is formed by the NW-SE extensional faults of the Carmel-Gilboa' zone. The central part of the block is dominated by open faults, flexures and minor faults. The small faults were measured in Limestone of Eocene age along the eastern and northern boundaries. These small faults as well as a few Neogene dikes indicate that one state of stress dominated the Gilboa' region since the Miocene with σ_H in WNW-ESE direction [Hatzor and Reches, 1990].

Stress Analysis of a Fault Cluster

The calculation of the stress tensor associated with slip along the faults in one cluster is performed in steps: recognizing the number of tectonic events, selecting the best solution and estimating the confidence margins. The method is demonstrated for one station marked here as GEVANW. This is a cluster of 30 faults measured in Triassic limestone layers in the northwest part of the Gevanim Dome, Ramon, southern Israel. The local inclination of the layers is up to 20° toward the northwest. The Gevanim dome developed due to a

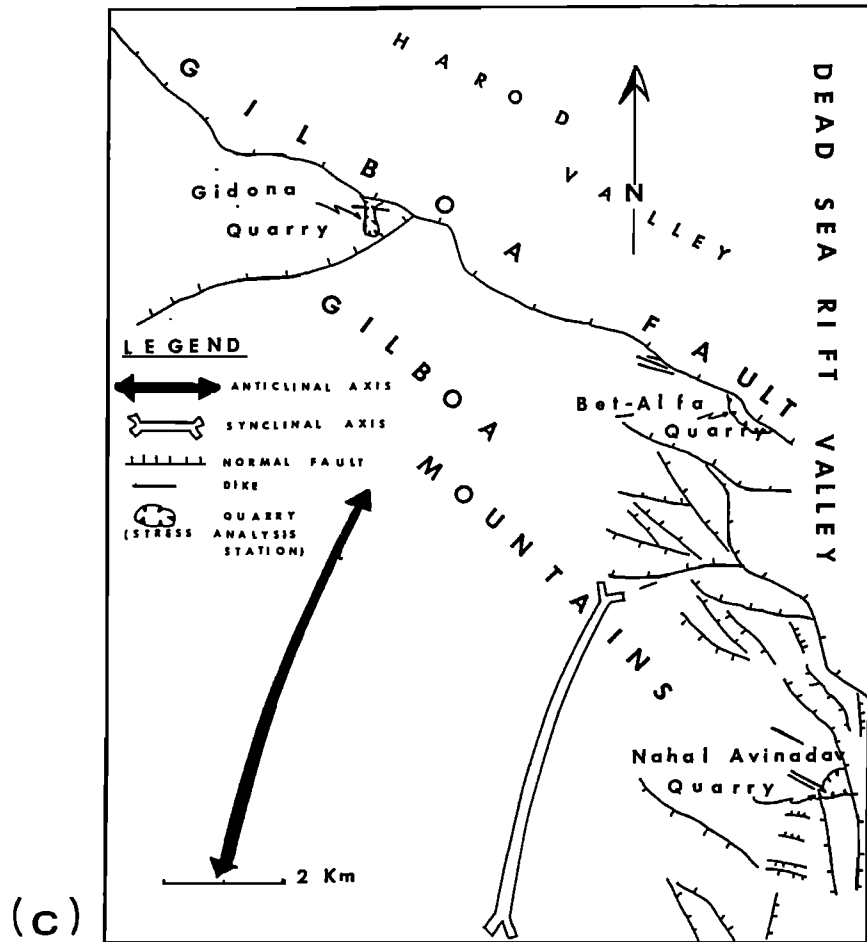


Fig. 2. (continued)

central laccolithic intrusion during the Early Cretaceous, and it was later amplified by regional compressive stresses [Baer and Reches, 1989]. The faults and their corresponding slip axes were rotated to the horizon around the strike of the host layers.

Number of tectonic phases. Suppose that a few different stress phases activated the faults measured in one area. The group of faults associated with one of the phases is regarded as a subset. It is reasonable that the misfit angles calculated for one subset which slipped under one state of stress will be significantly smaller than the misfit angles calculated for a mixture of a few subsets. This effect is demonstrated for the GEVANW cluster for which the inversion of all 30 faults yielded large SM and PAM (Figure 3a). We examine the possibility to reveal the separate tectonic phases by using two methods. First, by inspection, the faults reveal two orientation groups, one group of 21 steep faults with subhorizontal slip that strike E-W to NW-SE, and another group of nine dip-slip faults with strikes in the NW quarter (Figure 4a).

Separation on the basis of fault orientation is possible if distinct sets are observed or if definite cross cutting relations are detected. Frequently, such conditions do not exist, and therefore, we propose another separation method which utilizes the misfit angles calculated by the stress inversion. The method is applied in an interactive manner as shown in the following section for GEVANW.

The solution for all 30 faults shows large misfit angles (Figure 3a). Eight faults with $SM > 35^\circ$ apparently do not fit the general solution and should be separated first (Figure 3a); the PAM diagram does not indicate a clear separation into subsets (Figure 3a). After these eight

faults are separated, the stress tensor is recalculated for the other 22 faults. This procedure was repeated two more times until the discrimination of 18 faults as a well-defined subset with small misfit angles (Figure 3b). The original cluster of GEVANW was split into a primary subset of 18 faults and a secondary subset of 12 faults. The separation process is repeated for the secondary subset and a few more faults may be deleted; for GEVANW, four of the faults were rejected as they did not fit any solution.

Stereoplots of the faults and the slip axes are displayed in Figure 4. The primary subset includes one set of oblique right-lateral faults (Figure 4c), and the secondary subset includes eight oblique dip slip faults (Figure 4e). This separation and the calculated stresses (Table 2) are similar, even though not identical, to the separation by inspection (above). The structural analysis of the paleostresses in Ramon Domes [Baer and Reches, 1989], indicates that the primary subset represents the younger tectonic phase of Upper Cretaceous to Miocene age. The secondary subset belongs to the older phase, associated with the emplacement of the central intrusion during the Early Cretaceous.

Selecting the best fitted friction and stress solution. The next step is to select the best friction coefficient and the best stress tensor. The friction is part of the coefficients of the unknown stress components (equation (6b)) in the initial set of equations (equation 5b). The system of linear equations (equation 6a) is solved by substituting a "chosen" value of μ . This solution is repeated for the range of reasonable friction values from $\mu = 0.0$ to $\mu = 2.0$, usually in 0.1 increments. Thus, for each cluster, up to 20 separate stress solutions

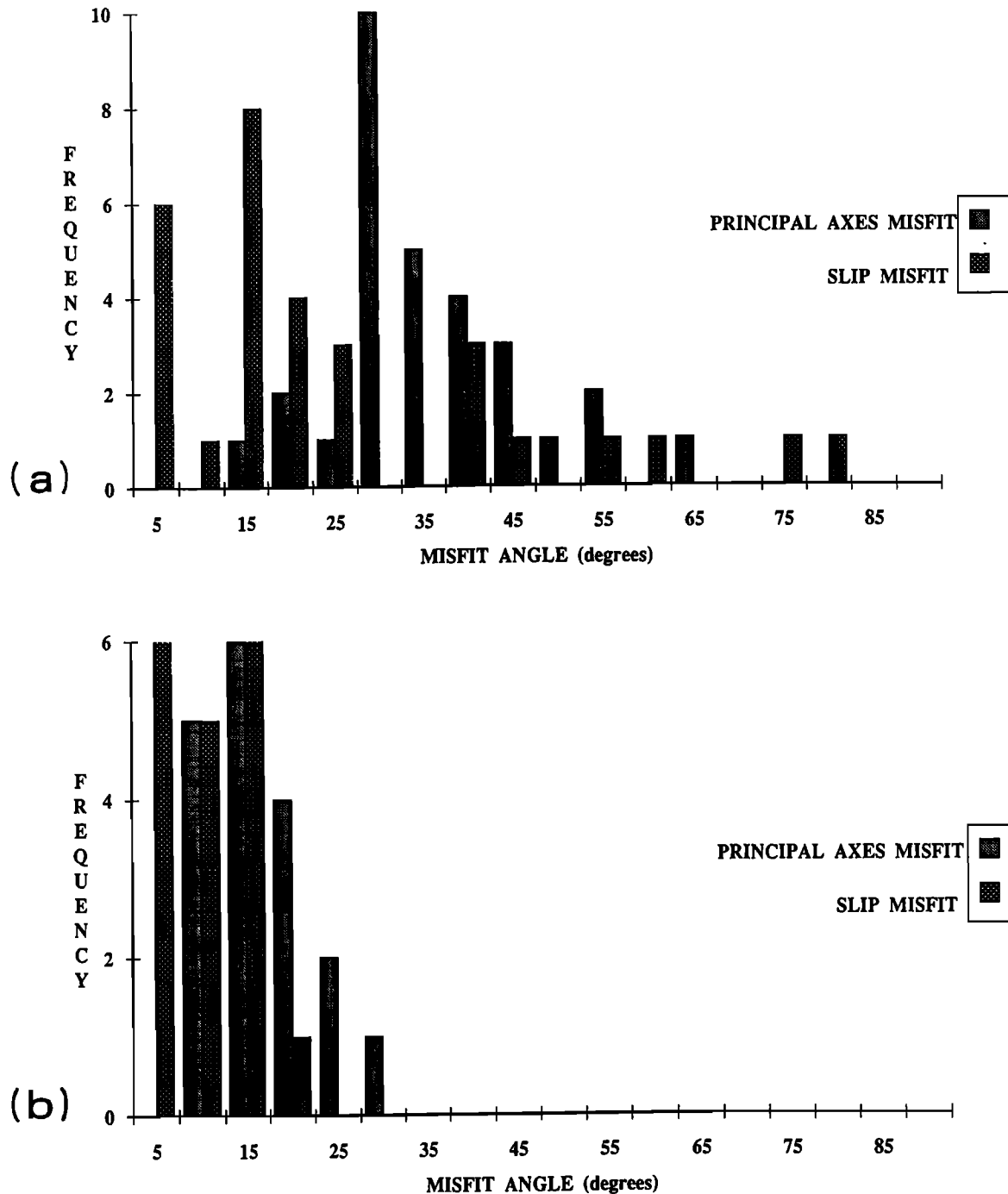


Fig. 3. The misfit angles calculated for the GEVANW fault cluster, Gevanim Dome, southern Israel. (a) Slip misfit, SM, and principal axes misfit, PAM, for all 30 faults measured in the field. (b) SM and PAM for the primary file of 18 faults.

are calculated; each solution with different friction value and different misfit angles. In most stress solutions of small faults the principal axes misfit PAM attains a single minimum value for the range $0.0 < \mu < 2.0$. We consider the stress solution with the least PAM and its corresponding friction as the best solution and the best friction, namely, the stress tensor and friction which best fit slip along all faults in the cluster.

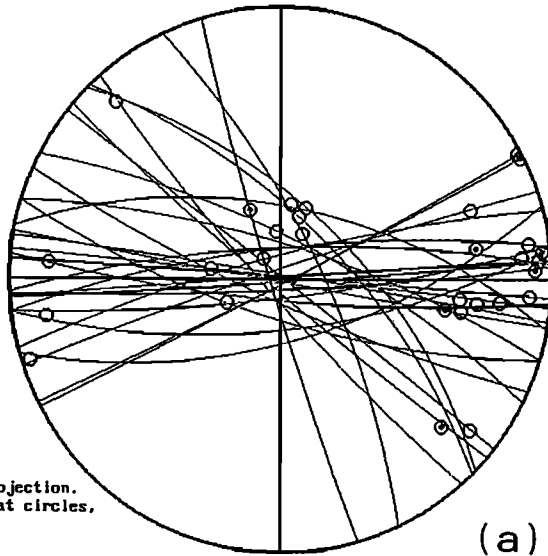
The results of these calculations for GEVANW are displayed in Table 2 and Figure 5. The best solution (smallest PAM) of the primary subset is for $\mu = 0.5$ (Figure 5a). The solution with the least value of PAM for the second subset is for $\mu = 1.9$ (Figure 5b).

However, the calculated normal stresses across two of the faults in this solution are tensile stresses; the derivation of tensile normal stresses is a frequent situation for high values of friction coefficients. We regard these solutions as unacceptable for reasons discussed above. Nevertheless, the calculated stress tensors for the secondary set of GEVANW indicate clear conditions of normal faulting for all friction coefficients (Table 2). In the present study, four clusters out of the 27 were rejected and their friction values are not included in the final analysis

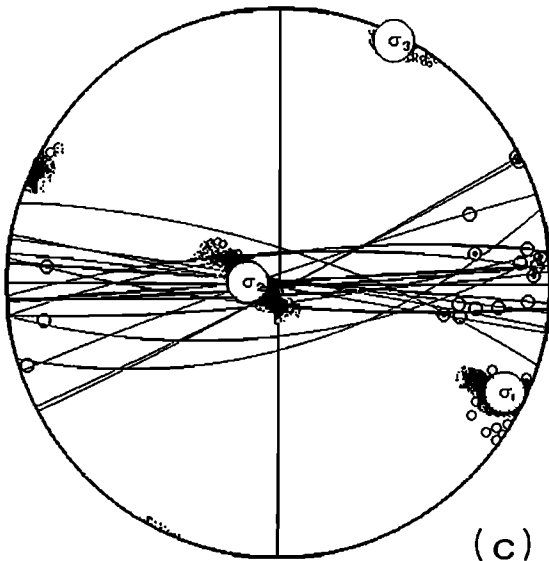
The confidence margins. The confidence margins are determined by the sampling-with-replacement method presented above.

SLIP AXIS
 Normal slip ○
 Reverse slip ⊙

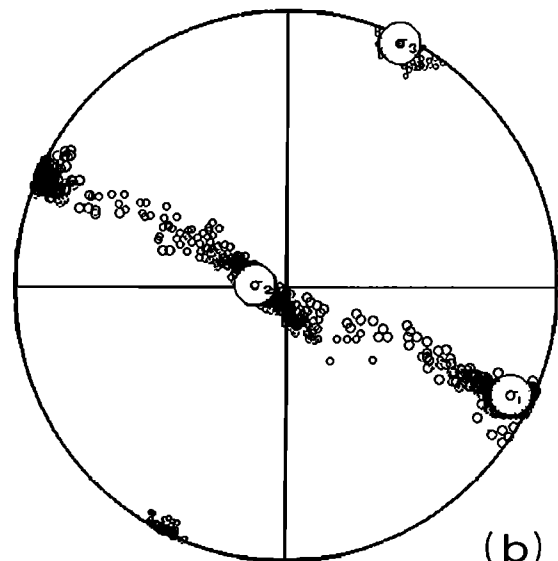
Equal angle,
 Lower hemisphere projection.
 Planes shown as great circles,
 Results of NW



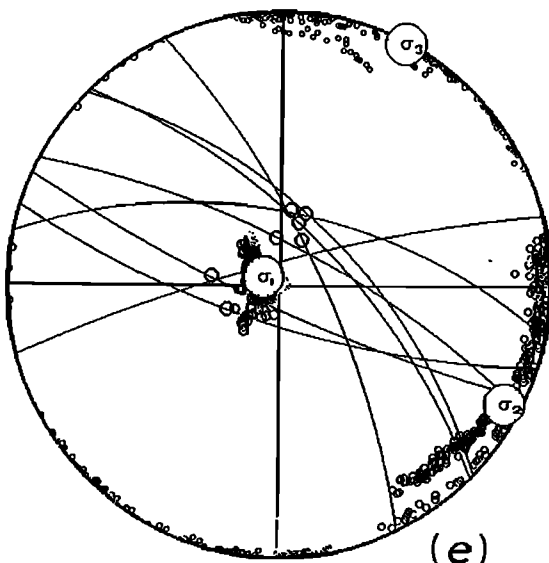
(a)



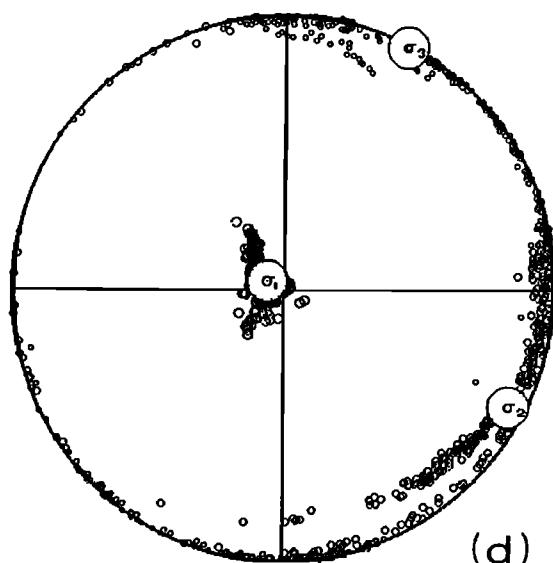
(c)



(b)



(e)



(d)

TABLE 2. Stress Inversion Results for GEVANW Fault Cluster, Measured in Northwest Area of Gevanim Dome, Ramon, Israel

Friction coeffi.	Misfit angles ^a		Magnitude ^b of the principal stresses			Stress ratio	Orientations of the principal stresses		
	PAM	SM	σ_1	σ_2	σ_3		σ_1	σ_2	σ_3
Primary Subset 18 Faults									
0.0	14.4	7.61	1.01	1.00	0.99	0.70	1/306	81/203	7/36
0.1	14.2	7.74	1.07	1.00	0.86	0.70	0/304	83/213	6/34
0.2	14.1	7.93	1.13	1.00	0.73	0.69	1/122	84/228	5/31
0.3	14.0	8.25	1.18	1.00	0.62	0.68	3/119	84/246	4/29
0.4	13.9	8.67	1.24	1.00	0.53	0.67	5/117	83/261	3/27
0.5	13.9	9.15	1.28	1.00	0.44	0.66	7/115	82/272	3/24
0.6	14.0	9.74	1.32	0.99	0.37	0.66	9/113	80/278	2/22
0.7	14.1	10.6	1.34	0.99	0.31	0.66	11/111	78/282	1/21
0.8	14.4	11.7	1.34	0.98	0.25	0.67	14/109	75/284	1/19
0.9	14.9	12.9	1.32	0.97	0.2	0.68	18/108	71/285	0/17
1.0	15.7	14.3	1.29	0.95	0.16	0.70	22/106	67/285	0/16
1.1	16.8	16.1	1.25	0.93	0.12	0.71	28/105	61/284	0/15
Secondary Subset, Eight faults									
0.0	42.1	22.1	1.00	0.98	0.97	0.26	76/300	8/169	9/77
0.2	23.4	10.5	1.00	0.61	0.59	0.06	86/329	2/119	1/210
0.4	18.6	9.90	1.00	0.42	0.39	0.05	86/312	3/111	1/201
0.6	14.9	9.39	1.00	0.31	0.27	0.06	85/290	4/107	0/197
0.8	13.3	8.85	1.01	0.25	0.19	0.07	84/276	5/107	1/17
1.0	12.7	8.26	1.01	0.20	0.14	0.07	83/273	6/110	1/19
1.2	12.1	7.79	1.01	0.15	0.10	0.05	82/281	7/112	1/22
1.4	11.2	7.47	1.01	0.11	0.08	0.03	82/298	7/113	0/203
1.6	10.7	7.03	1.02	0.07	0.06	0.01	82/313	7/113	2/203
1.8	10.5	6.53	1.02	0.05	0.05	0.00	81/323	7/108	4/199

a, in degrees
b, normalized by the effective vertical stresses.

Figure 4 shows the principal stress axes calculated for 500 subsidiary clusters selected from the original sets. The principal axes of the subsidiary clusters are marked by small circles; they form three clouds around the principal axes of the best solution. The angular deviations of the stress solutions of the 500 subsidiary clusters have normal distribution around the best solution. Thus 68.27% of the additional solution are within the range of ± 1 s. d. from the best solution. Figures 4c and 4e display 68.27% of the solutions which are the closest to the best solution for the primary and secondary subsets; these clouds of solutions bound the range of ± 1 s. d.

DISCUSSION

Coefficients of Friction

The stress inversion calculations were applied to the 27 fault clusters in the procedure described above for GEVANW. For each cluster the calculations were performed with friction coefficients which range from $\mu = 0.0$ to $\mu = 2.0$. The magnitudes of the principal axes misfit angle, PAM, vary with the friction coefficients in a manner similar to GEVANW subsets (see above, Figures 4 and 5 and Table 2). The selected friction coefficient for each cluster is the one which corresponds to the least PAM.

Acceptable solutions (see rejection criterion above) were obtained to 23 clusters out of the 27 analyzed (Table 1). The selected friction coefficients range from 0.0 to 1.3 with mean value of 0.58 ± 0.37 (Table 1 and Figure 6a). This friction coefficient appears in general agreement with the experimental friction of Byerlee's law (equations 2). Thus the analysis supports, in general, the common strength estimates of the upper crust [e.g., *Brace and Kohlstedt, 1980*].

While the calculated friction values are scattered over a wide range, more than half of them (12) have values of 0.4–0.6 (Figure 6a). The scattering of the friction values is apparent for the different tectonic region (Figure 6b) and does not appear to be related to the rock type (Table 1).

One possibility for the data scattering is the depth of faulting as experimental work shows that the friction coefficients are scattered in experiments with normal stresses smaller than 5 MPa [Byerlee, 1978]. In these experiments the friction varies from 0.3 to 10.0, in contrast to the consistent values for larger normal stresses [Byerlee, 1978, Figure 3]. The normal stress σ_n , acting on faults in the field is most likely bounded by $0.5\sigma_{\text{vertical}} < \sigma_n < 1.5\sigma_{\text{vertical}}$. Thus 5 MPa of normal stress corresponds to 125–375 m depth for rock density of 2,500 kg/m³. The faults analyzed here slipped at somewhat deeper levels. The faults in the Gilboa' block were measured in Eocene

Fig. 4. Stereoplots of the faults, slip axes and calculated stress tensors in GEVANW station. Sense of slip is marked on the plot of the slip axes according to the legend. Principal stress axes are marked as σ_1 , σ_2 and σ_3 ; lower hemisphere, equal area projection. (a) Stereoplot of the faults measured in the field, 30 faults. (b) Stress solution for the primary subset of 18 faults with 500 bootstrapping solutions (see text) marked by small circles forming three clouds about the principal axes. (c) Same as Figure 4b with the projected faults and with ± 1 s. d. margins (see text). (d) Stress solution for the secondary subset of eight faults with 500 bootstrapping solutions (see text) marked by small circles forming three clouds about the principal axes. (e) Same as Figure 4d with the projected faults and with ± 1 s. d. margins (see text).

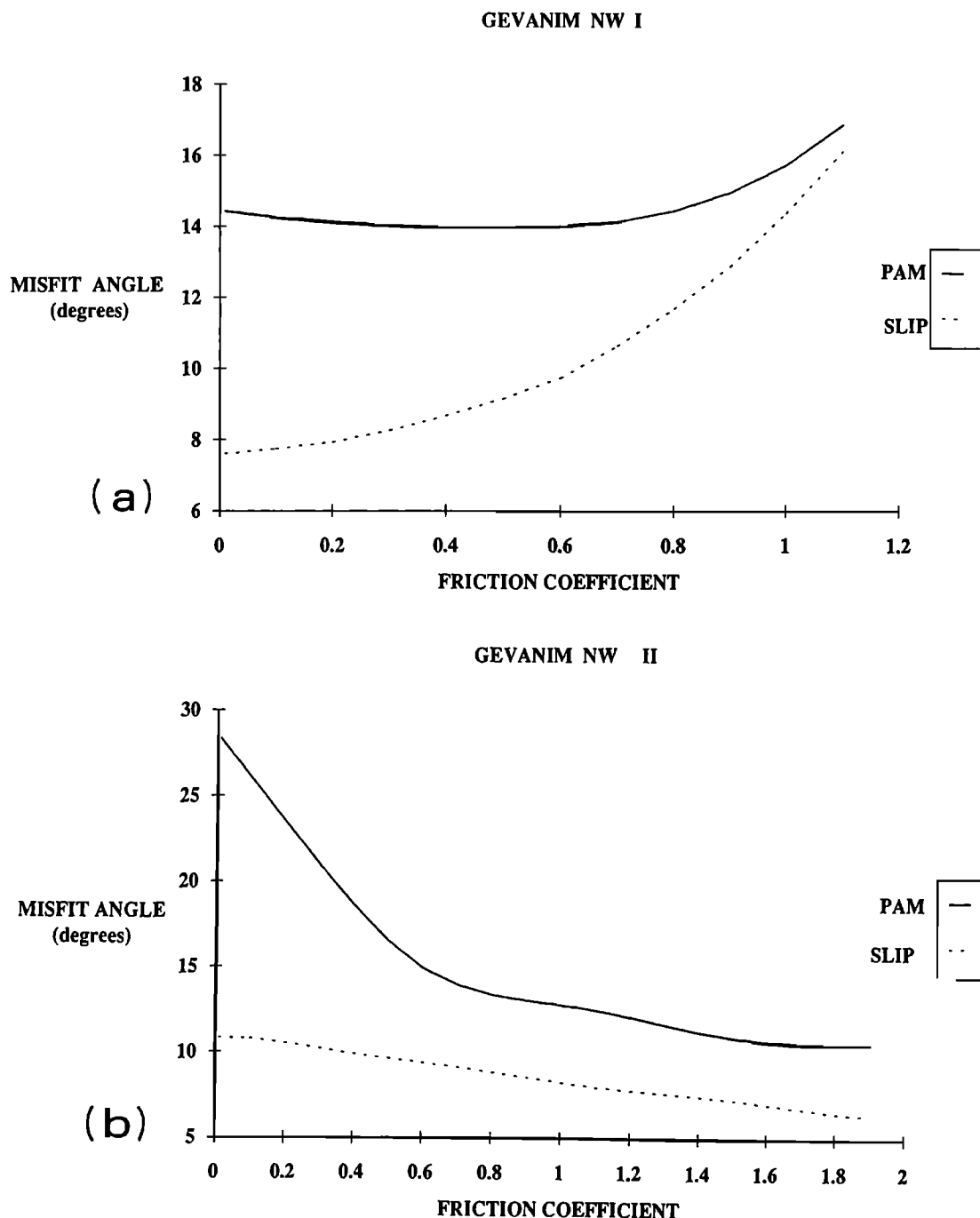


Fig. 5. Calculated misfit angles versus the selected coefficients of friction for GEVANW cluster, Ramon. Solid curve, principal axes misfit angle, PAM; dashed curves, slip misfit angle, SM. (a) The primary subset (18 faults). (b) The secondary subset (eight faults).

rocks, with maximum overburden of few hundred meters [Hatzor, 1988]. The faulting in Ramon domes occurred under maximum overburden of about 1 km [Baer and Reches, 1989]. Most of the faults measured in the Grand Canyon area, are related to the Laramide tectonism [Reches, 1978] and slipped at a likely depth of about 2 km. Thus the scatter of the friction coefficients can only partly be explained by Byerlee's experimental results for low normal stress.

The scatter of the friction may also indicate a genuine variations of friction in the field, possibly related to properties of the fault surfaces. However, the limited number of cases and rock types at the present analysis precludes the deduction of more refined conclusions.

Magnitude of the Tectonic Stresses

The magnitudes of the tectonic stresses were estimated in several studies of stress inversion [Gephart and Forsyth, 1984; Michael, 1984; Angelier, 1989]. The first step in these studies was to calculate a reduced stress tensor, presented by the ratio of the principal stress axes $\phi = (\sigma_2 - \sigma_3) / (\sigma_1 - \sigma_2)$. The selected tensor was the one which minimizes the slip misfit angle (see above). Gephart and Forsyth [1984] and Michael [1984] used the reduced stress tensor to inspect whether their selected failure criterion is satisfied along each of the observed faults. Angelier [1989] proposed to evaluate the magnitude of the tectonic stresses by linking friction, rock strength, and field

FRICITION CALCULATED BY STRESS INVERSION

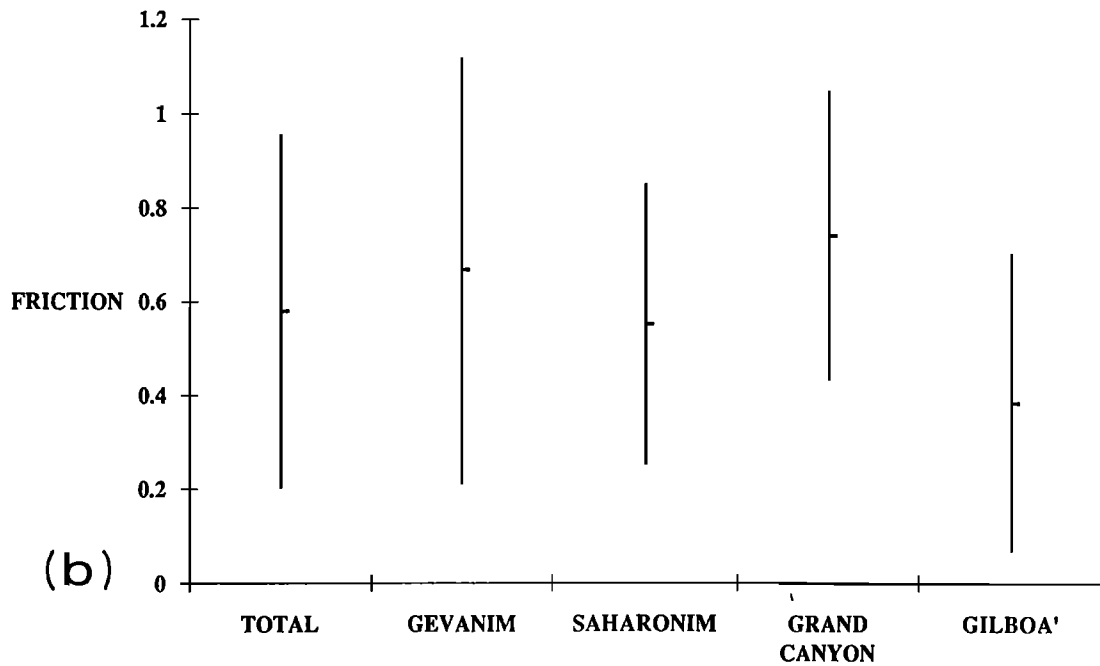
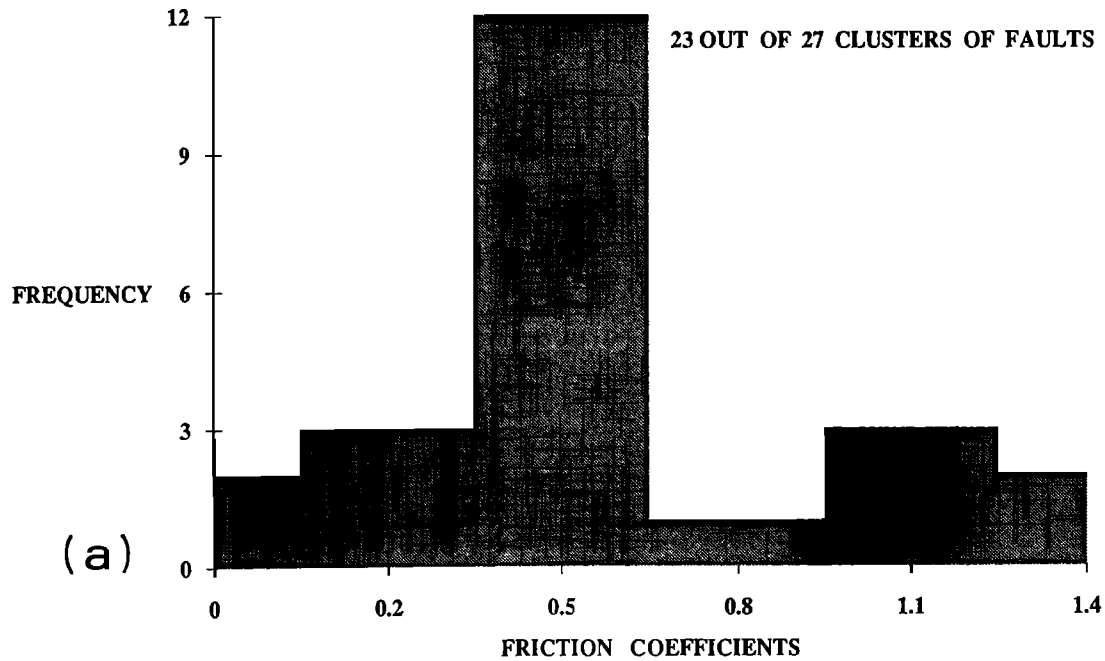


Fig. 6. (a) Frequency of the coefficient of friction estimated for the analyzed clusters. Best fitted friction for 23 out of 27 clusters analyzed. (b) The mean friction coefficients ± 1 s. d. calculated for the four different groups of faults and the total.

observations. First, he estimated the friction from the shear stress/normal stress ratio determined from the reduced stress tensor; then he evaluated the stress magnitude from neoformed conjugate faults, laboratory determined parameters of rock strength, and estimates of depth of faulting.

In this section we compare the magnitudes of the principal stresses calculated for the clusters in Table 1, with the measured magnitudes of in situ tectonic stresses. The fault clusters are divided into groups with similar states of stress and groups from the same location (Table

3). The purpose of this division is to estimate the variations of the stress magnitudes between stations. The first group includes nine clusters from Ramon domes which consist mostly of strike-slip faults. The second group includes two clusters from the Grand Canyon area which consist mostly of strike-slip faults. The third group includes the five clusters of strike-slip faults from the Gilboa' block. The fourth group includes four clusters from Ramon domes and one from the Grand Canyon which consist mostly of normal faults. A single cluster with prevailing reverse faults (GC263403,

TABLE 3. Magnitudes of the Principal Stresses Shown as Fraction of the Vertical stress, Including the Pore Fluid Pressure

Fault Type, Locations	Number of faults	σ_1 / σ_v	σ_2 / σ_v	σ_3 / σ_v
I. Strike slip faults				
A. Ramon, ^a	9	1.40 ± 0.23	0.95 ± 0.08	0.54 ± 0.24
B. Grand Canyon, ^a	2	2.72 ± 0.10	0.98 ± 0.01	0.71 ± 0.14
C. Gilboa ^a	5	1.25 ± 0.21	1.00 ± 0.01	0.77 ± 0.22
D. Rangely, Colorado, ^b		1.98	1.00	0.33
II. Normal faults				
E. Ramon, ^a	5	1.06 ± 0.08	0.42 ± 0.34	0.36 ± 0.366
F. Nevada Test Site, ^c		≈ 1.00		≈ 0.50

a, present work

b, Raleigh et al., [1972]

c, Zoback and Healy, [1984]

Table 1) is not included in the present discussion as it was not possible to estimate the standard deviation of its stress magnitude in comparison with other similar clusters.

The principal stresses calculated in the present method are the effective principal stresses normalized by the vertical effective stress (equation (9)). Even though the stresses presented in Table 3 were calculated for past faulting events, the magnitudes of these paleo-stresses are similar to the magnitudes of recently measured tectonic stresses. We selected two cases to portray this similarity: the Rangely anticline, Colorado [Raleigh et al., 1972], and the Nevada Test Site [Zoback and Healy, 1984]. The stresses of the two cases are listed in Table 3 as stress ratios, $\sigma_i / \sigma_{\text{vertical}}$, to facilitate the comparison with the stress ratios of the inversion calculations.

The in situ stresses in Rangely anticline, Colorado, were studied due to the local earthquakes induced by the variations of the pore fluid pressure [Raleigh et al., 1972]. The total stresses were $\sigma_{\text{HMAX}}=59$ MPa, $\sigma_v=42.7$ MPa and $\sigma_{\text{HMIN}}=31.4$ MPa; the pore fluid pressure at the depth of the stress experiments is about 26 MPa. The ratios of the effective stresses, $(\sigma_{\text{HMAX}}-P_p)/(\sigma_v-P_p)$ and $(\sigma_{\text{HMIN}}-P_p)/(\sigma_v-P_p)$, are listed in Table 3. The normalized magnitudes of the effective principal stresses calculated for the strike-slip faults in the present study cover a wide range (fault types A, B, and C in Table 3), which appears to include the corresponding in situ stresses in Rangely Anticline (fault type D in Table 3).

The Nevada Test Site is in a state of incipient normal faulting, in which the least tectonic stress is horizontal, and it is approximately equal to one half of the vertical stress [Zoback and Healy, 1984] (fault type F in Table 3). In a region of normal faulting where σ_1 is the vertical load, an increase of the shear stresses can be achieved by the reduction of σ_2 and σ_3 . Thus the value of $\sigma_3 \approx 0.5 \sigma_v$ in Nevada is an upper bound on the least horizontal stress in that region. The calculated least stress of $\sigma_3 \approx 0.36 \sigma_v$ for group E of the present study (normal faults) is smaller than the measured least stress in Nevada. This smaller stress most likely indicates large shear stress during actual faulting in Ramon, versus smaller shear stress during incipient, pre faulting stage in Nevada.

It is illustrated above that the stresses calculated in the present inversion method are similar in relative magnitudes of in situ stresses in two selected locations (Table 3). This similarity suggests that the

stress inversion method has the potential to determine the in situ stresses for recent earthquakes and ancient faults.

SUMMARY

1. The stress inversion method presented here and by Reches [1987] determines the tectonic stress tensor associated with simultaneous slip along many faults in a cluster. The quality of the solution is evaluated by the misfit angle of the principal axes. This is the mean angle between the stress axes of the tensor calculated for the entire cluster, and the stress axes of the ideal tensor calculated for each fault. The most suitable solution is the one with the minimum value of this misfit angle.

2. The coefficients of friction of the most suitable solutions have mean value of 0.58 ± 0.37 (Figure 6). This value is in general agreement with the experimental value of 0.6 to 0.85 compiled by Byerlee [1978, equations 2]. The wide scatter of the calculated friction probably indicates shallow depth of faulting.

3. The magnitudes of the principal stresses calculated for the strike-slip faults and normal faults measured in several sites in Israel and the Grand Canyon, Arizona, appear to be in reasonable agreement with the magnitudes of in situ stresses measured in Rangely Anticline and Nevada Test Site.

Acknowledgments. We have benefitted from the discussions with J. Gephart and A. Michael. The comments and suggestions of B. Ellsworth, J. Gephart, and T. Herring significantly contributed to the paper. The study was supported in part by the US-Israel Binational Science Foundation, grant 86-183.

REFERENCES

- Angelier, J., Tectonic analysis of fault slip data sets, *J. Geophys. Res.*, **89**, 5835-5848, 1984.
- Angelier, J., From orientation to magnitudes in paleostress determinations using fault slip data, *J. Stru. Geol.*, **11**, 37-50, 1989.
- Baer, G., and Z., Reches, Tectonic stresses, igneous intrusions and structural development of two domes in Ramon, southern Israel, *Tectonophysics*, **166**, 293-315, 1989.
- Brace, W. F., and D. L., Kohlstedt, Limits on lithospheric stress imposed by laboratory experiments, *J. Geophys. Res.*, **85**, 6248-6252, 1980.
- Bott, M. H. P., The mechanics of oblique slip faulting, *Geol. Mag.*, **96**, 109-117, 1959.

- Byerlee, J. D., Friction of rocks, *Pure Appl. Geophys.*, 116, 615-626, 1978.
- Carey, E., and B. Bruiner, Analyse theorique et numerique d'un modele mecanique lementaire applique a l'etude d'une population de failles, *C. R. Hebd. Seances. Acad. Sci., Ser. D*, 279, 891-894, 1974.
- Efron, B., *The Jackknife, the Bootstrap and Other Resampling Plans*, 92 pp., SIAM, Philadelphia, Pa., 1982.
- Ellsworth, W.L., A general theory for determining the state of stress in the Earth from fault slip measurements, *Terra Cognita*, 2(2), 170, 1982.
- Gephart, J. W., and D. W. Forsyth, An improved method for determining the regional stress tensor using earthquake focal mechanism data: Application to the San Fernando earthquake sequence, *J. Geophys. Res.*, 89, 9305-9320, 1984.
- Hatzor, Y., The geology of the Gilboa' region, M. Sc. thesis, (in Hebrew with English abstract), Hebrew Univ., Jerusalem, 107 p., 1988.
- Hatzor, Y., and Z., Reches, Structure and paleostresses in the Gilboa' region, western margins of the central Dead Sea rift, *Tectonophysics*, 180, 87-100, 1990.
- Jaeger, J. C. and N. W. G. Cook, *Fundamentals of Rock Mechanics*, 2nd ed., 513 pp., Methuen, New York, 1976.
- Kirby, S., Rheology of the lithosphere, *Rev. Geophys.*, 21, 1458-1487, 1983.
- McGarr, A., and N.C., Gay, State of stress in the Earth crust, *Annu. Rev. Earth Planet. Sci.*, 6, 404-436, 1978.
- Michael, A. J., Determination of stress from slip data: Faults and folds, *J. Geophys. Res.*, 89, 11,517-11,526, 1984.
- Raleigh, C. B., J. H., Healy and J.D., Bredehoeft, Faulting and crustal stress at Rangely, Colorado, in *Flow and Fracture of Rocks, Geophys. Monog. Ser.*, vol. 16, edited by Heard H. C., I. Y., Borg, N. L., Carter, and C. B., Raleigh, pp. 275-284, AGU, Washington D. C., 1972.
- Reches, Z., The development of monoclines, Part I: Structure of the Palisades Creek branch of the east Kaibab monocline, Grand Canyon, Arizona, in *Laramide Folding Associated With Basement Block Faulting in the Rocky Mountain Region*, edited by V. Matthews, *Mem. Geol. Soc. Am.*, 151, 235-278, 1978.
- Reches, Z., Determination of the tectonic stress tensor from slip along faults that obey the Coulomb yield criterion, *Tectonics*, 6, 849-861, 1987.
- Stuart, A., *The Ideas of Sampling*, 91 pp., C. Griffin, High Wycombe, 1984.
- Zoback, M. D., and J. H., Healy, Friction, faulting and in situ stress, *Annu. Geophys.*, 2, 689-698, 1984.

G. Baer, Geological Survey of Israel, 30 Malkhe Street, Jerusalem, 95501, Israel.

Y. Hatzor, Department of Civil Engineering, University of California, Berkeley, CA 94720.

Z. Reches, Department of Geology, Hebrew University, Jerusalem, 91904, Israel.

(Received October 2, 1989;
revised September 19, 1990;
accepted October 13, 1990.)